energies

Article

Energy Efficiency of a Solar Wall with Transparent Insulation in Polish Climatic Conditions

Jadwiga Świrska-Perkowska *, Andrzej Kucharczyk and Jerzy Wyrwał

Department of Physics of Materials, Faculty of Civil Engineering and Architecture, Opole University of Technology, Katowicka 48, 45-061 Opole, Poland; a.kucharczyk@po.edu.pl (A.K.); j.wyrwal@po.edu.pl (J.W.)
* Correspondence: j.swirska-perkowska@po.edu.pl; Tel.: +48-77-449-8554

Received: 16 January 2020; Accepted: 13 February 2020; Published: 16 February 2020

Abstract: A numerical model of a solar wall (SW) with transparent insulation (TI) is proposed in this article. The model is based on the finite-difference method and thermal conductivity equation, with a heat source term for the absorber. Using this model, the energy efficiency of a solar wall with transparent insulation (SW-TI) with honeycomb insulation made of modified cellulose acetate was analyzed in the case of different climatic conditions prevailing in Poland, different orientations of the envelope, and different insulation thicknesses. Simulations were carried out throughout the whole heating period. Monthly energy balances and temperature distributions for the analyzed envelopes at individual moments of the heating period are the basic results of the simulations. It was found that the use of 108 and 88 mm thick insulation was the most recommended in the considered temperate climate. Placing transparent insulation on a wall with an eastern or western orientation caused the annual heat balance of the envelope to decrease by 24–31% in relation to the value of this balance in the case of a southern orientation. The monthly heat balances obtained using the proposed model give results consistent with the method of calculating heat gains for opaque building envelopes with transparent insulation included in the PN-EN ISO 13790:2008 standard.

Keywords: transparent insulation; energy efficiency; Polish climate; temperate climate

1. Introduction

Buildings currently account for around 40% of the global energy use. In this balance, it should be taken into consideration that residential buildings consume around 35% for heating and ventilation, and public buildings consume up to 45% for heating [1]. In order to reduce the energy consumption of buildings and increase the thermal comfort in rooms, the requirements for the energy efficiency of buildings are becoming increasingly stringent. This is connected to the successive reduction of permissible heat transfer coefficients of building envelopes and increasing their airtightness. In practice, this usually means increasing the thickness of standard thermal insulation, which results in an increase in wall thickness of up to 50 cm and a reduction in the usable area of the building in relation to its floor plan [2].

Therefore, solar walls with transparent insulation (TI) are becoming an increasingly interesting design option for new low-energy buildings and renovating passive buildings [3,4]. The solar wall is used to convert solar radiation energy, based on a passive system employing a heat-accumulating layer for indirect energy gain. This layer is made of high-density material (e.g., ceramic bricks, sand-lime blocks, and ordinary concrete). An absorber is placed on the outer wall surface with glazing or transparent insulation. Transparent insulation is a material characterized by high solar radiation transmission (usually above 40%) and increased thermal insulation (however, several times less than in the case of materials usually used for thermal insulations of buildings). TI not only performs the same function as conventional insulation, reducing heat loss from rooms, but also allows solar radiation to be transmitted at a level of 50% [3], while demonstrating low infrared losses. The passive solar wall is designed to allow solar energy to be stored in order to reduce energy consumption for heating. The thermal accumulation layer of the envelope stores heat during the sunny part of a day and transfers it to the interior of the building with some delay. In this case, larger heat losses are compensated by heat gains in comparison to walls with conventional insulation, and the solar wall acts as a heat source in the room.

The concept of insulating the external walls of buildings with transparent insulation materials (TIM) was developed more than 30 years ago [3]. Since then, experimental work has been conducted to demonstrate the effectiveness of different TIMs. The results of the demonstration projects carried out under the International Energy Agency's program have been reported [5–7]. Experiments on real objects equipped with TI are described in articles [8–12], while in works [13,14], a test room was used to determine the thermal efficiency of an opaque wall covered with a TIM. In all the above mentioned works, a decrease in the heat demand for the heating of buildings with the use of TI on the external building envelopes was observed, as well as the danger of the overheating of rooms during the summer period.

The conducted studies show that a well-designed solar wall (SW) requires a massive layer for heat accumulation, a shading device for protection against overheating in the period of a high solar radiation intensity, and a southern orientation [5,6]. At this point, it should be mentioned that the appropriate orientations of the walls equipped with transparent insulation may be from east through south to west; however, a southern orientation is preferred. The reduction of excessive solar gains can also be achieved by using appropriate selective absorbers [15–17] and thermotropic layers integrated with transparent insulation, which reversibly reduce the total solar energy transmittance, becoming opaque after heating [10]. Works [3,18–20] provide an overview of insulation systems based on transparent materials, as well as the materials which transparent insulations are made of.

In order to analyze the influence of changes in design parameters on the thermal efficiency of solar walls, a sensitivity analysis is carried out. The most frequently used methodology in the analysis of the efficiency and sensitivity of solar heating walls is based on numerical simulations [18,21]. Compared to studies of a scaled model, such simulations are more cost-effective, both in terms of time and finance, as changes in TI parameters can be easily incorporated into a computer program and thus provide guidance on how to optimize future applications [3]. At present, many building simulation tools, such as EnergyPlus, ESP-r, and TRNSYS, have been adapted to calculate the energy efficiency of buildings using transparent insulation [3,19].

The behavior of building envelopes containing transparent insulation can be predicted using various calculation models and approximation methods. Thermal processes occurring in such envelopes can be simulated dynamically over long periods of time (e.g., year and heating season), considering them as part of the building which they belong to. Then, the previously mentioned computer programs may be used effectively for such calculations [17,22,23]. To estimate the impact of transparent insulated envelopes on the thermal balance of a building, simplified stationary algorithms, such as the one proposed in [4] or the "Un-Utilizability Design Method" [24,25] used in [21,26], are utilized. For a shortened analysis of transient heat conduction within an envelope during one day, a simplified model based on electrical analogies and the finite-difference method can be used [27,28]. Such an approach allows the behavior of a solar wall in a period of days with different insolation to be analyzed and the daily heat gains or losses in the given conditions to be determined.

Despite the numerous advantages of transparent insulations, there are still barriers to be overcome before their widespread use. One of them is the fact that construction practices differ significantly from country to country, so building design strategies should take into account significant regional differences in climate patterns [17]. Therefore, despite the numerous studies already carried out on solar walls, more work needs to be done to gain knowledge about their behavior and to optimize them according to the specificity of each climate region [29].

This article presents a numerical model of a solar wall with transparent insulation (SW-TI). This model was obtained from discretization (in accordance with the idea of the finite-difference method) of the thermal conductivity equation in which the source terms corresponding to the absorption of solar radiation by the absorber and radiation heat transfer between the surfaces limiting the air gap between the absorber and the insulation were introduced. The convective heat transfer within this gap is taken into account in a simplified way by increasing the thermal conductivity of air by multiplying by the Nusselt number (this is acceptable for Nu values less than or equal to 1.2 [30]).

As a result of the proposed approach, it was possible to divide the analyzed envelope into small spatial elements (more than 60 nodes), which improves the accuracy of calculated finite differences, introduces equal distances between spatial nodes (4 mm) in all wall layers, and maintains the condition of continuity of heat fluxes at the contact of these elements. For comparison, in article [27], in which the finite-difference method is used to adopt electrical analogies, envelope discretization is performed with only 11 nodes and the insulation itself with two nodes lying on its external surfaces. A similar approach to the problem can be found in paper [28], in which six nodes were introduced in the accumulation layer of the envelope, completely omitting the thermal capacity of transparent insulation (TI is taken into account by adding its resistance to the resistance of heat transfer on the external surface of the wall). The above mentioned numerical models do not give the possibility to obtain temperature distributions in the analyzed envelope. They only allow the temperature values at a few selected node points to be determined.

The purpose of the simulations carried out in the article was also to assess the energy efficiency of an SW-TI for various climatic conditions prevailing in Poland, i.e., with high, medium, and low insolation. For each case, the simulation was carried out for the whole heating period (from September to May), with different thicknesses of transparent insulation (68, 88, 108, and 128 mm) and with different wall orientations (east, south, and west). It was assumed that transparent insulations are equipped with appropriate sunscreen roller-blinds that will protect the building against overheating during the summer period. Hence, the calculations were not performed for the months from June to August. As a result, temperature distributions in the envelopes at various moments of the process and their energy balances, both in individual months and in the whole heating period, were obtained. The results were compared with those obtained using the stationary method of calculating thermal gains through opaque envelopes with transparent insulation included in the PN-EN ISO 13790:2008 standard. The equivalent heat transfer coefficient of an SW-TI in individual months of the heating period and its efficiency were also determined. Preliminary considerations in this area, using a simplified calculation model neglecting convection and radiation in the air gap, regarding only 108 mm thick insulation and a southern orientation of the envelope, were presented in [31]. The results of these analyzes inspired the authors to conduct further intensive research on this issue.

The calculations carried out allow conclusions on the legitimacy of using SW-TI within the territory of Poland, as well as guidelines for designers on the thickness of applied insulation and the preferred orientation of solar walls, to be drawn. The main purpose of the research was to assess the suitability of solar-accumulating walls equipped with transparent insulation in Polish climatic conditions and to encourage designers to use this solution in all regions with a similar temperate climate. The intention of the work was also to present a new approach to modeling thermal phenomena occurring in SW-TI partitions.

2. Materials and Methods

2.1. Analyzed Partition

This study analyzed an envelope with transparent honeycomb insulation and a density of 16 kg/m^3, made of modified cellulose acetate, and placed between two panes with a thickness of 4 mm (TIMax CA). The material used in the insulation is resistant to short-term influences of temperature of 140 °C and long-term influences of temperature of 100 °C [32]. Four variants of insulation thickness were considered: 68, 88, 108, and 128 mm. Table 1 presents the coefficients of solar energy permeability and thermal parameters of the applied insulation. The values of the effective thermal conductivity coefficient of cellulose acetate panels presented in the paper were calculated on the basis of the heat transfer coefficient U given by the manufacturer, assuming that the thermal conductivity coefficient of the glazing was 1.0 W/(m·K).

Table 1. Properties of transparent insulation.

Insulation Thickness (mm)	The τ_{TI} Factor of the Whole Set (-)	The U Coefficient of the Whole Set (W/(m^2·K))	The λ Coefficient of the Honeycomb Panel (W/(m·K))
68	0.62	1.3	0.079
88	0.59	1.0	0.081
108	0.56	0.8	0.081
128	0.53	0.6	0.072

The analyzed SW-TI envelope consisted of the following layers (Figure 1):

- Transparent insulation;
- Non-ventilated air gap of a 20 mm thickness;
- Sand-lime blocks with a thickness of 240 mm, density of 1800 kg/m^3, specific heat of 880 J/(kg·K), and thermal conductivity of 0.65 W/(m·K);
- Cement-lime mortar with a thickness of 12 mm.

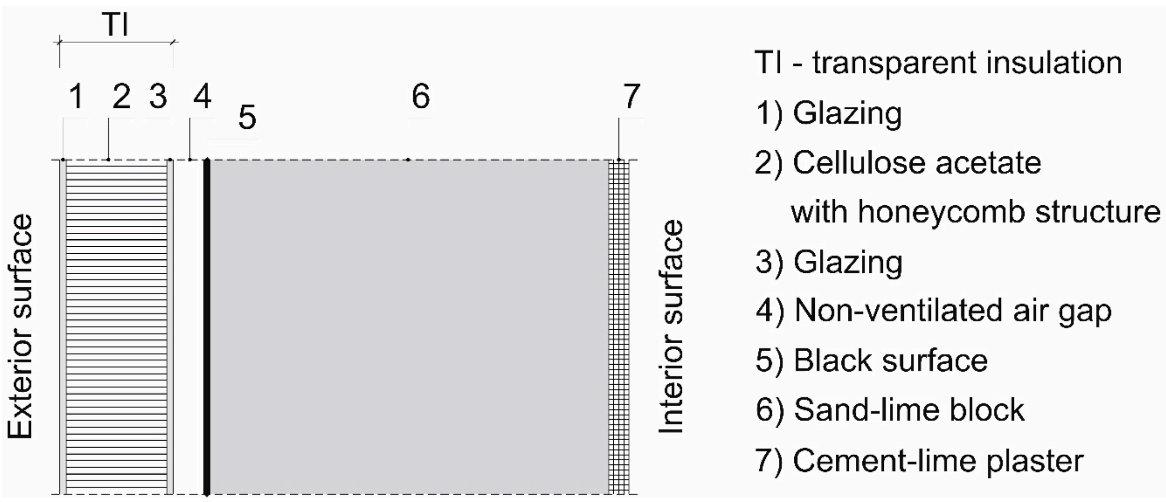

Figure 1. The analyzed solar wall with transparent insulation.

It was assumed that, on the side of transparent insulation, blocks are covered with black paint with a solar radiation absorption coefficient of 0.94. It was also assumed that transparent insulations are equipped with appropriate sunscreen roller-blinds that will protect the building against overheating during the summer period.

2.2. Climatic Data

The SW-TI thermal efficiency depends on various factors that can be generally divided into two categories: construction and location, and climate. The first group includes factors such as the type of insulation, its glazing, heat-accumulating layer material, and its properties, as well as orientation and shading. The second category includes parameters describing the climate within which the intensity of solar radiation and external temperature are the most important factors [31].

The Polish climate is defined as temperate and transitional between the warm, maritime climate of western Europe and the continental one covering Ukraine and Russia. According to the Köppen classification, the Polish climate belongs to the Dfb type, i.e., it is a humid continental climate with warm summers and precipitation evenly distributed throughout a year. The average annual insolation on a horizontal surface in Poland is typically in the range of 950 to 1150 kWh/m^2 (in comparison with Germany, a country neighboring Poland, where it ranges from 930 to 1300 kWh/m^2, and in France, where it ranges from 1000 to 1900 kWh/m^2). The highest insolation occurs in June (160 kWh/m^2 for Warsaw), while the irradiation at the lowest level occurs in the month of December (monthly average insolation is 11 kWh/m^2). In the winter period, from October to March, only 20% of the total annual radiation reaches the ground [33].

The intensity of solar radiation, its variability in time, and its availability in different locations have a decisive meaning for the efficiency of SW-TI and other devices using solar energy. In truth, differences in insolation in Poland are not too great; however, more and less sunny areas can be distinguished [33]. The highest level of insolation is observed in south-eastern and southern Poland, while in northern Poland, the solar irradiation is the lowest.

In this article, the energy efficiency of transparent insulation installed on the eastern, southern, and western wall of a building is analyzed. Their locations are assumed in three selected cities, i.e., in Racibórz, Poznań, and Koszalin. The annual insolation on a horizontal surface is as follows [34]: Racibórz—1086 kWh/m^2 (southern Poland), Poznań—961 kWh/m^2 (central Poland), and Koszalin—827 kWh/m^2 (northern Poland). All three considered locations have winter and summer climatic severity indexes (WCSI and SCSI, respectively) at a level that allows them to qualify for climate zone E1 (WCSI $>$ 1.51 and SCSI $<$ 0.5) [35]. These indexes are, respectively, Racibórz—WSCI = 2.26, SCSI = 0.11; Poznań—WSCI = 2.47, SCSI = 0.15; and Koszalin—WSCI = 2.38, SCSI = 0.04. The comparisons of the solar irradiation on a horizontal surface and average outdoor temperature in particular heating period months for the considered locations are presented in Figure 2.

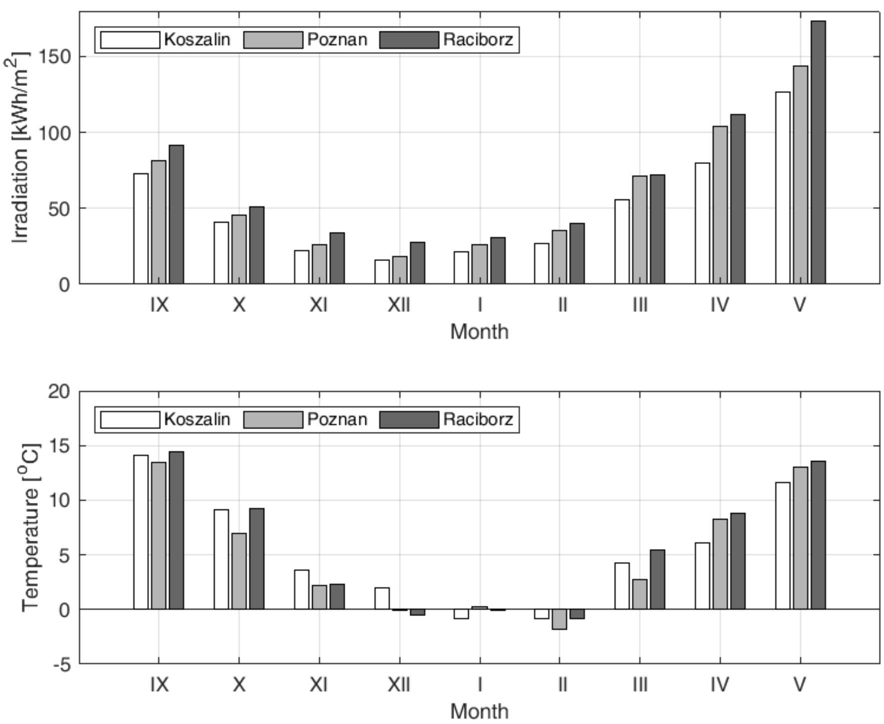

Figure 2. The irradiation on a horizontal plane (top graph) and average outdoor temperature (bottom graph) in particular months of the heating season.

A set of hourly meteorological parameters corresponding to a given location and describing, in numbers, a typical meteorological year, were the input data for the calculations. They were downloaded from the website of the Ministry of Funds and Regional Policy [34], from the tab containing climatic data for Poland which, among others, is intended for preparing energy performance certificates for buildings. The parameters used in this article are hourly values: solar radiation intensity (in W/m^2), external temperature (in °C), and wind speed (in m/s) over the entire heating period in the case of the considered cities. The variabilities of these quantities are shown illustratively for Poznań in Figures 3 and 4.

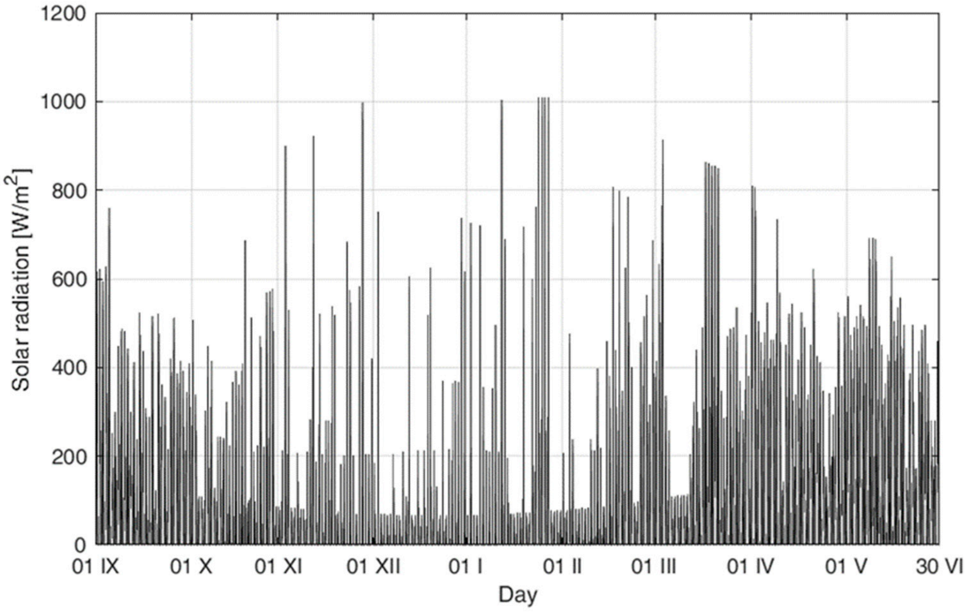

Figure 3. The intensity of solar radiation falling on the vertical plane in Poznań during the heating period.

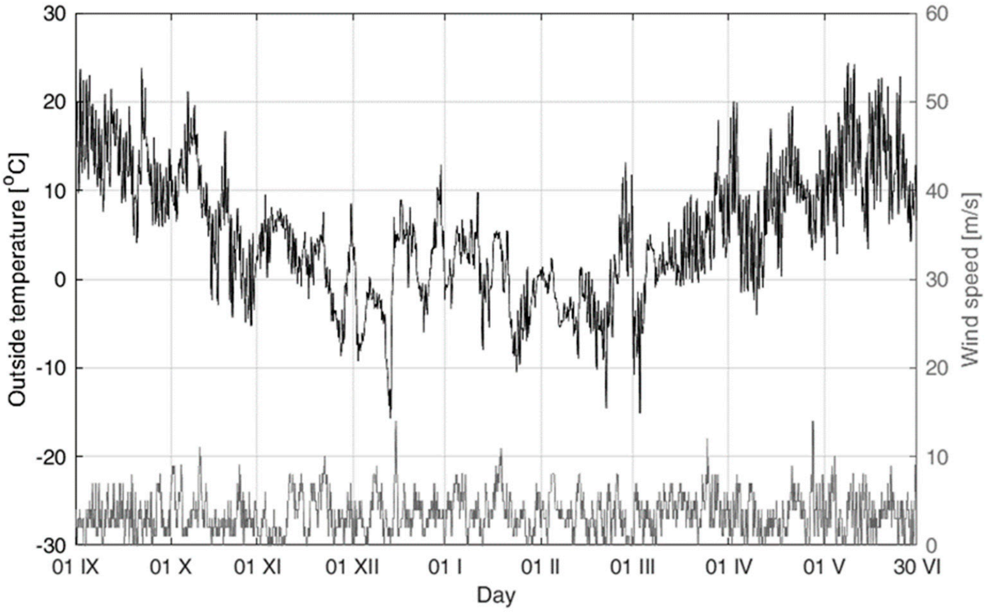

Figure 4. The outside temperature and wind speed in Poznań during the heating period.

2.3. Governing Equations and Assumptions

In the finite-difference method, there is a problem with meeting the conditions for the continuity of fluxes at the boundaries of layers at points where solar radiation absorption occurs (additional heat flux). This difficulty is usually avoided by introducing an additional flux into the thermal conductivity equation at the place where solar radiation is absorbed [27,28]. Then, in order to obtain a numerical model of the analyzed issue, the method of elementary balances [36] or resistor analogue [27,28] is usually used. A possible solution to this problem is to introduce source terms into the thermal conductivity equation. In this study, the second of these solutions has been used, assuming that the analyzed issue concerns non-stationary one-dimensional heat transport with source terms at the location of the absorber. Appropriate source components were also introduced on the surfaces, limiting the air gap, to take into account the radiation heat exchange between these surfaces. It was assumed that the adsorption of solar radiation by transparent insulation glass shields is negligibly low and that the convective heat exchange in the air gap would be taken into account by increasing the thermal conductivity of the air accordingly (multiplied by the Nusselt number).

In the above approach, the analyzed problem is described by the following system of differential equations:

- The thermal conductivity equation:

$$\rho c \frac{\partial \Theta}{\partial t} = \lambda \frac{\partial^2 \Theta}{\partial x^2} + Q_{sol} + Q_{rad}, \quad Q_{sol} = \frac{\alpha_{sol,abs} \tau_{TI} I_{sol}}{d_a}, \quad Q_{rad} = \frac{q_{rad}}{d_{rad}}; \tag{1}$$

- The boundary conditions on the inner and outer surface of the envelope:

$$-\lambda \frac{\partial \Theta}{\partial x} = \beta_e(\Theta(0,t) - \Theta_e(t)), \tag{2}$$

$$-\lambda \frac{\partial \Theta}{\partial x} = \beta_i(\Theta_i - \Theta(l,t)); \tag{3}$$

- The initial condition:

$$\Theta(x,0) = \Theta_o(x), \tag{4}$$

where Θ—temperature (°C), ρ—material density (kg/m^3), c—specific heat (J/(kg·K)), λ—thermal conductivity coefficient (W/(m·K)), x—spatial coordinate (m), t—time (s), Q_{sol}—heat source in the envelope (occurring at the location of the absorber) (W/m^3), Q_{rad}—heat source related to radiation heat exchange (occurring at the places where planes limit the air gap) (W/m^3), $\alpha_{sol,abs}$—coefficient of absorption of solar radiation by the absorber (usually greater than 0.9) (-), τ_{TI}—coefficient of total transmittance of solar radiation energy of transparent insulation (-), I_{sol}—intensity of total solar radiation falling on the envelope surface (W/m^2), d_a—arbitrary thickness of the absorber (part of the envelope absorbing solar radiation) (m), q_{rad}—radiative heat flux (J/(s·m^2)), d_{rad}—arbitrary thickness of part of the envelope absorbing radiative heat flux (m), β—convective heat transfer coefficient (W/(m^2·K)), Θ_o—initial temperature (°C), l—envelope thickness (m), and subscripts e and i—external and internal.

In the above equations, it was assumed in a simplistic way that all material coefficients occurring in the model are constant, except for the air parameters, which were calculated at each analyzed moment of the process in order to precisely determine the Nusselt number. However, it was assumed that the variation of these parameters over time is negligibly small compared to the temperature changes. It was further assumed that the coefficient of convection heat transfer on the external surface of the envelope depends on the wind speed and is equal to [37]

$$\beta_e = 4w + 5.6 \quad \text{if} \quad w \le 5\,\text{m/s}, \tag{5}$$

$$\beta_e = 7.1 w^{0.78} \quad \text{if} \quad w > 5\,\text{m/s}, \tag{6}$$

where w is the wind speed and the heat transfer coefficient on the internal surface of the envelope is constant and equal to β_i = 7.69 (W/(m^2·K)).

The radiative heat flux occurring in Equation (1), which is exchanged between two surfaces, limiting the air gap, can be calculated from formula [38]:

$$q_{rad} = C\varepsilon_{eff}\left(T_a^4 - T_{gl}^4\right), \tag{7}$$

where T_a and T_{gl}—temperature of the absorber and the inner cover plate of the transparent insulation, respectively (K); $C = 5.67{\cdot}10^{-8}$ (W/(m$^2{\cdot}$K^4))—blackbody radiation constant (Stefan–Boltzmann constant); and ε_{eff}—effective emissivity (–), which can be calculated for two infinite parallel surfaces:

$$\varepsilon_{eff} = \frac{1}{\frac{1}{\varepsilon_a} + \frac{1}{\varepsilon_{gl}} - 1}. \tag{8}$$

In Formula (8), ε_a and ε_{gl} denote the emissivity of the absorber (0.94) and emissivity of the glass surface (0.836), respectively [39].

In this paper, the discrete model of the problem was obtained directly by the discretization of Equations (1)–(3), using right-sided differential quotients for temporal discretization and central quotients for the calculation of spatial derivatives. In this way, an open difference scheme was constructed in which temperatures at individual points over the next time step $\Theta_{i,j+1}$ were determined directly from the knowledge of temperatures in the previous step [36]. Discredited equations, taking into account that we are dealing with a multi-layered medium, take the form of

$$\begin{aligned} \frac{\rho_i c_i + \rho_{i+1} c_{i+1}}{2} \frac{\Theta_{i,j+1} - \Theta_{i,j}}{\Delta t} \\ = \frac{2\lambda_{i+1}}{\Delta x_{i+1}(\Delta x_i + \Delta x_{i+1})}\left(\Theta_{i+1,j} - \Theta_{i,j}\right) \\ - \frac{2\lambda_i}{\Delta x_i(\Delta x_i + \Delta x_{i+1})}\left(\Theta_{i,j} - \Theta_{i-1,j}\right) + \frac{\alpha_{sol,abs}\tau_{TI} I_{sol,i,j}}{\Delta x_i} + \frac{q_{rad,i,j}}{\Delta x_i}, \end{aligned} \tag{9}$$

$$\lambda_0 \frac{\Theta_{1,j} - \Theta_{-1,j}}{2\Delta x_i} = \beta_e\left(\Theta_{0,j} - \Theta_{z,j}\right) \to \Theta_{-1,j} = -\frac{2\beta_e \Delta x_i}{\lambda_0}\left(\Theta_{0,j} - \Theta_{e,j}\right) + \Theta_{1,j}, \tag{10}$$

$$\lambda_n \frac{\Theta_{n+1,j} - \Theta_{n-1,j}}{2\Delta x_n} = \beta_i\left(\Theta_{i,j} - \Theta_{n,j}\right) \to \Theta_{n+1,j} = \frac{2\beta_i \Delta x_i}{\lambda_0}\left(\Theta_{i,j} - \Theta_{n,j}\right) + \Theta_{n-1,j}, \tag{11}$$

where indexes i and j refer to spatial and temporal discretization, respectively; n is the number of nodes in the envelope; and indexes -1 and $n + 1$ refer to the fictional nodes. In Equation (9), it is assumed that $d_a = d_{rad} = \Delta x_i$. This means that a given flux is absorbed by the part of the envelope represented by the node i. The impact of such an assumption on the solution obtained will be analyzed in point 2.5 of the article.

For the open scheme, there is a limitation in the length of the time step Δt. The condition of algorithm convergence was that the factor occurring in Equation (9) for $\Theta_{i,j}$ was positive. Hence, at the constant Δx_i, we can get the condition

$$1 - \frac{\Delta t}{\rho_i c_i}\left(\frac{\lambda_i + \lambda_{i+1}}{(\Delta x)^2}\right) \geq 0 \to \Delta t \leq \frac{\rho_i c_i (\Delta x)^2}{\lambda_i + \lambda_{i+1}}. \tag{12}$$

In the case of the analyzed envelope, the biggest limitation in the length of the time step results from the fact that there is an air gap of small values ρ and c, for which the above condition is met (at $\Delta x = 4$ mm) for $\Delta t \leq 0.167$ s.

2.4. Convective Heat Transfer

The convective heat exchange within the rectangular air gaps caused by the difference in temperature between the vertical walls limiting the gap can be quantified by the convective heat transfer coefficient β. This coefficient is usually a function of various independent variables (e.g., temperature difference) in a dimensionless form [40]. The contribution of convective heat transport to the total heat transfer can be expressed by the Nusselt number (*Nu*), which is the ratio of the total transmitted flux by conduction and convection to the value of the conductive heat flux:

$$Nu = \beta l/\lambda = q/q_{cond} \Rightarrow q = Nu\ q_{cond}, \tag{13}$$

where l is the width of the gap, and q and q_{cond} are total and conductive heat fluxes, respectively.

The Nusselt number is a function of the Rayleigh number (*Ra*), Prandtl number (*Pr*), and gap shape factor (A) (the ratio of its height to its width, $A = H/l$). Since the value of the Prandtl number for gases never significantly differs from 0.71, its influence on the Nusselt number is negligible [40], hence,

$$Nu = Nu(Ra, A). \tag{14}$$

The Rayleigh number describes the fluid movement caused by the difference in density. It takes into account the physical properties of the fluid in the heat exchange process through natural convection [40]:

$$Ra = \frac{gl^3\gamma\Delta T}{\mu a} = \frac{gl^3\Delta T}{\mu a T_{av}}, \quad a = \frac{\lambda}{\varrho c}, \gamma \cong \frac{1}{T_{av}}, \tag{15}$$

where g—gravitational acceleration (m^2/s), γ—coefficient of thermal expansion of the fluid (1/K), ΔT—temperature difference in the gap (K), T_{av}—average temperature in the gap (K), μ—coefficient of kinematic viscosity (m^2/s), and a—thermal diffusivity (m^2/s). If the Rayleigh number is below the critical value for a given fluid, the heat transfer mainly occurs by conduction, and if this value rises above the critical value, the heat transfer mainly occurs by convection [41].

The air parameters in dependencies (15) can be calculated from the following formulas [42]:

$$\rho = \rho_o(1 - \gamma(T - T_o)), \tag{16}$$

$$\mu = \left(5{\cdot}10^{-8}T + 2{\cdot}10^{-6}\right)/\rho, \tag{17}$$

$$\lambda = 8{\cdot}10^{-5}T + 1.6{\cdot}10^{-3}, \tag{18}$$

$$c = 0.07T + 985.5, \tag{19}$$

where T_o—reference temperature (K) and ρ_o—air density at reference temperature.

Each curve $Nu(Ra)$ starts on the left hand side (at $Ra = 0$) at $Nu = 1$ and increases with the increase in the *Ra* value. If $Nu = 1$, the total heat flux value is equal to that which would exist if the gas was stagnant and energy was transmitted only through conduction. This is called a conduction regime. At higher values of *Ra*, the convective transfer rate is greater and *Nu* is rising. Apart from the conduction regime, with the further growth of *Ra*, there is a transitional regime, followed by a regime of the border layer. The conduction regime is controlled by conduction, the transitional regime by near wall conduction and convection in the core, and the boundary layer regime by core convection and conduction limited to a relatively thin boundary layer near the walls. The critical value of *Ra*, at which the transfer leaves the conduction regime, is a function of A. Convection transfer leaves the conduction regime at lower values of *Ra* in gaps with lower values of A [41].

The value of the Nusselt number for convection in the rectangular air gap can be determined from the formulas [43]

$$Nu = max(Nu_1, Nu_2, Nu_3), \tag{20}$$

$$Nu_1 = 0.0605Ra^{1/3}, \tag{21}$$

$$Nu_2 = \left(1 + \left(\frac{0.104Ra^{0.293}}{1 + \left(\frac{6310}{Ra}\right)^{1.36}}\right)^3\right)^{1/3}, \tag{22}$$

$$Nu_3 = 0.242\left(\frac{Ra}{A}\right)^{0.272} \quad A = \frac{H}{l}. \tag{23}$$

As can be seen from the above expressions, only the size Nu_3 is dependent on the shape factor A, and only affects the Nusselt number in cases where $A < 25$ [40].

Experimental studies have shown that the Nusselt number rises quite slowly with Ra until it reaches 1.2, after which it grows quite rapidly. Accordingly, when the value of Nu is equal to or less than 1.2, it can be assumed that convection is suppressed, there is pure heat transfer by conduction in still air, and its value is increased by $(Nu - 1)\cdot 100\%$ [27]. Therefore, in the discussed case, the occurrence of heat convective lifting can be taken into account by multiplying the heat conduction coefficient by the value of the Nusselt number.

2.5. Model Verification and Validation

First of all, the convergence of the algorithm was checked. For this purpose, calculations for the time steps 0.18, 0.09, and 0.045 s were performed. It was found that the average of temperature differences determined at each spatial point and time moments, corresponding to the 12th and 24th hour of the day at the middle and end of each month, amounted to 1.29×10^{-5} °C for $\Delta t = 0.18$ s and $\Delta t = 0.09$ s, and the maximum difference was 1.06×10^{-4} °C. The analogous average, determined when changing the time step from 0.09 to 0.045 s, was 6.45×10^{-6} °C, with the maximum difference of 5.54×10^{-5} °C. In the latter case, no noticeable differences were found in the monthly heat balances for the envelope determined for particular time steps. It was found that the algorithm was convergent, and all calculations were further carried out for $\Delta t = 0.09$ s.

Then, it was checked whether the assumption of $Nu \leq 1.2$ in the analyzed envelope was met. For this purpose, during all simulations, the average and maximum values of Nu were determined, and the time, when Nu increased above 1.2, was calculated (if such a case occurred). It was found that the average value of the Nusselt number, calculated for the whole heating season in the case of all analyzed insulation thicknesses, locations, and orientations of the solar wall, was within the range of 1.0013 to 1.0142, whereas the maximum value of this number was within the range of 1.0303 to 1.3037. A temporary exceeding the limit value of 1.2 was observed for all 88 and 68 mm thick insulation cases and for 108 mm thick insulation located in Racibórz facing south, with the maximum time period of 15.34 h for which this situation occurred, i.e., for 0.234% of the total duration of calculations. As a result of such minor and short-term exceeding, it was concluded that the assumption made could be considered to have been met.

It was also examined how the length of the spatial step Δx, occurring, i.a., in the denominator of source terms, influences the obtained solutions. For this purpose, the temperature distributions in the envelope with TI with a thickness of 108 mm at a harmonically changing outdoor temperature and radiation intensity were calculated:

$$I_{sol} = 900\, sin\left(\frac{3\pi t}{86400} - \pi\right), \tag{24}$$

$$\Theta_e = -0.6 + 6\, sin\left(\frac{2\pi t}{86400} - \frac{\pi}{2}\right). \tag{25}$$

The above conditions simulate a cloudless, very sunny January day, with an average temperature of −0.6 °C and an amplitude of 6 °C, lasting 8 h. Only positive values of I_{sol} were taken into account in the calculations. Simulations were carried out for $\Delta x = 4$ and 2 mm, and temperature distributions were recorded every hour. It was found that the average difference between temperatures calculated for the individual values of Δx was equal to 0.0036 °C, with a maximum difference of 0.0188 °C. At the same time, the daily energy balance of the envelope only changed by 2.3×10^{-5}%. Examples of temperature distributions for 10:00 a.m., 12:00 noon, and 2:00 p.m., obtained using both spatial steps, are shown in Figure 5. The same calculations were repeated at a solar intensity amplitude of 600 W/m^2. In this case, an average difference of 0.0029 °C, a maximum of 0.0183 °C, and a percentage change in the balance of 5×10^{-5}% were found. Therefore, it was assumed that the modification of Δx considered does not affect the final result, which is the energy balance of the envelope in the individual months of the heating season, and all calculations were carried out at a space step of 4 mm.

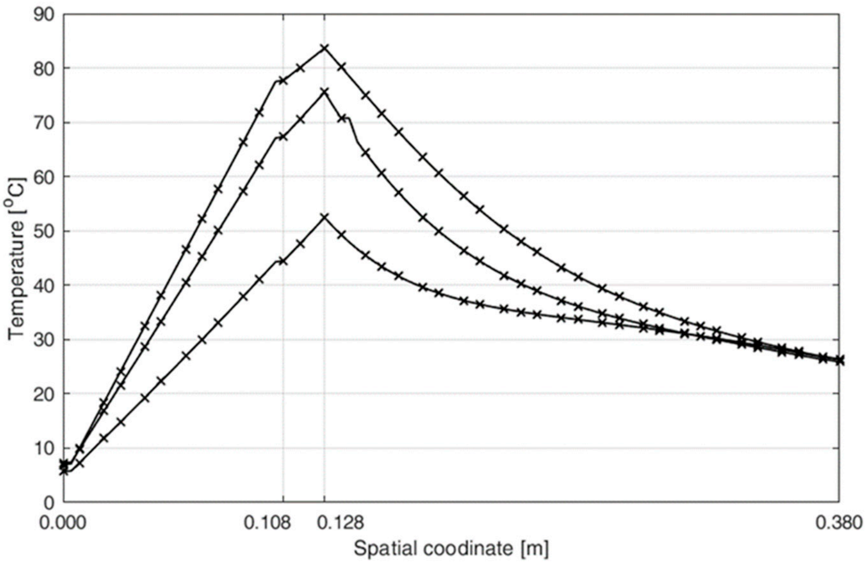

Figure 5. Temperature distribution in the envelope at 10:00 a.m., 12:00 noon, and 2:00 p.m. (from below) calculated at Δx = 4 mm (solid line) and at Δx = 2 mm (crosses).

Due to the lack of experimental data relating to the envelope under analysis, model validation was carried out on the basis of a stationary method for calculating heat gains for opaque envelopes with transparent insulation included in the PN-EN ISO 13790:2008 standard. According to this method, the solar gains for an unshaded SW-TI per m^2 of the wall can be calculated from the formula [44]

$$\Phi_{sol} = I_{sol,m}\alpha_{sol,abs}\tau_{TI}U/U_{te}, \quad U_{te} = 1/(R_{se} + R_{TI} + R_a), \quad R_{se} = 1/\beta_e, \tag{26}$$

where Φ_{sol}—monthly gains from transparent insolation (kWh/m^2), $I_{sol,m}$—monthly solar irradiation for a plane with a given orientation (kWh/m^2), R_{se}—heat transfer resistance on the external surface of the envelope (m^2·K/W), R_{TI}—thermal resistance of transparent insulation (m^2·K/W), and R_a—thermal resistance of the air gap (m^2·K/W).

By subtracting from Formula (26) the heat loss of the envelope in the month under consideration, we obtained the monthly heat balance Q_m of the solar wall. Such calculations were made for all analyzed cases of location and orientation of the SW-TI. The differences ΔQ_m between the monthly balances were then determined, which were estimated numerically and with the use of the standard method. The sum of the absolute values of these differences for the entire heating season was also calculated. By relating the value of the above sum to the sum of the absolute values of the balances calculated numerically, percentage discrepancies between these two methods were estimated:

$$e = \left(\sum_m |\Delta Q_m| / \sum_m |Q_m|\right) \cdot 100\%. \tag{27}$$

The average difference $\overline{\Delta Q_m}$ was determined for each case analyzed.

After analyzing the results obtained (e.g., Figures 6 and 7), it was concluded that average differences between values Q_m obtained from both methods were in the range of 0.3905 to 0.8675 kWh/m^2, while the relative difference was between 2.29% and 3.54% (except for the case of the envelope with 108 mm thick insulation located in Koszalin and oriented to the west, for which e had the value of 11.11%). Of course, the percentage differences calculated for the individual months, especially winter ones, had higher values of up to 40%. This is due to the fact that the heat balance values Q_m are low for these months. Hence, the differences in ΔQ_m at 0.2 kWh/m^2 caused a significant relative difference.

Considering the above, it was concluded that both methods show a high degree of convergence, and the proposed numerical model was found to be correct. It is worth noting at this point that this model, taking into account the dynamics of the thermal processes occurring, allows for a more accurate determination of the values of Q_m. This is particularly important for critical winter months, when heat gains are most desirable.

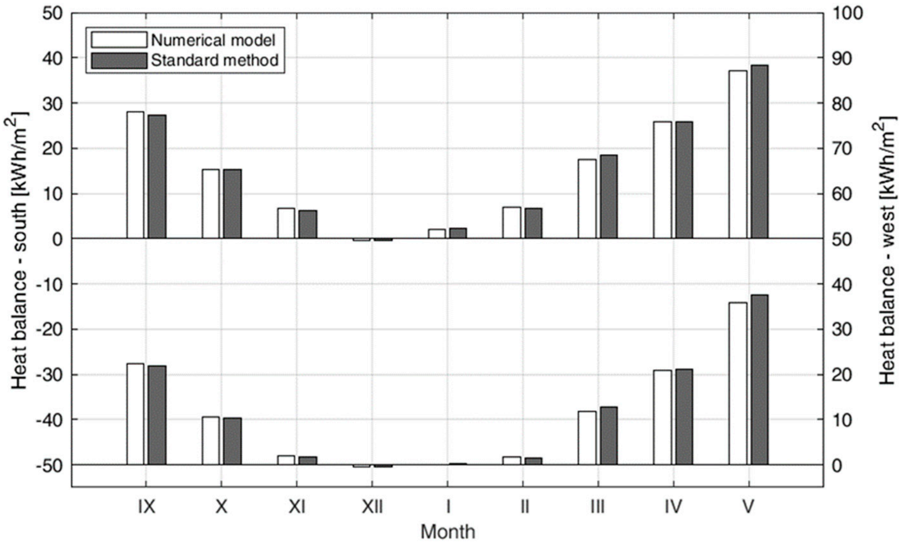

Figure 6. Comparison of results obtained using the standard method and a numerical model for Koszalin (top—south orientation and bottom—west orientation).

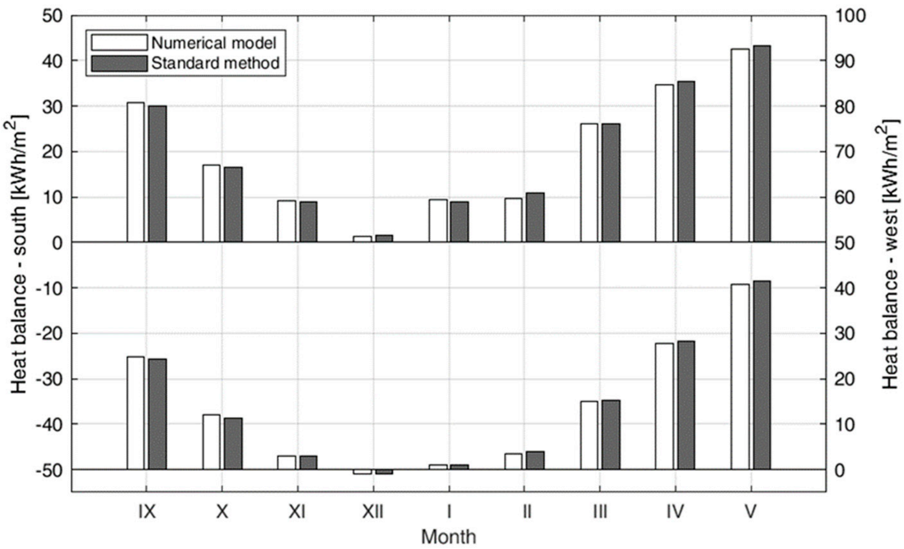

Figure 7. Comparison of results obtained using the standard method and a numerical model for Poznań (top—south orientation and bottom—west orientation).

3. Results

The program for thermal calculations was written by the authors in the Matlab environment. Simulations were carried out for an envelope with 108 mm thick transparent insulation and three different locations of the envelope (Koszalin, Poznań, and Racibórz), corresponding to low, medium, and high insolation, and three orientations of the SW-TI: east, south, and west. Additionally, for the south orientation, the calculations were carried out for all the considered locations for envelopes with transparent insulation of a 68, 88, and 128 mm thickness. In all the cases mentioned above, monthly energy balances of the wall were also determined using the standard method described in point 2.5.

The program also calculated the weekly and monthly average efficiency of envelopes in given conditions, defined as

$$\eta = \frac{\overline{q}_{is,sol} - \overline{q}_{is}}{\overline{I}_{sol}}, \tag{28}$$

where $\overline{q}_{is,sol}$—average value of the flux on the internal surface of the envelope, over a given period, taking into account solar gains (W/m^2); $\overline{q}_{is}$—average value of the flux on the internal surface of the envelope, over a given period, excluding solar gains (W/m^2); and $\overline{I}_{sol}$—average intensity of solar radiation over a given period.

The average values of equivalent heat transfer coefficients were also determined:

$$U_{eq} = \overline{\left(\frac{q_{is,sol}}{\Theta_i - \Theta_e}\right)}, \tag{29}$$

where the upper line indicates the average of the quantity in the brackets. The negative value of this coefficient is related to the predominance of envelope heat gains over losses. In this case, the wall becomes the source of heat in the room.

When modeling the envelope thermal behavior, insulation glazing and the transparent insulation itself were considered as separate layers. For this purpose, the envelope element was divided into 4 mm thick layers. This made it necessary to apply a time step of 0.09 s.

In the case under consideration, there is a problem with the initial condition because the temperature distribution in the envelope at the initial moment is not known. Therefore, the initial moment in the simulations corresponded to the day of August 1 under the assumption of a homogeneous boundary condition (Θ_o = 20 °C), and this part of the thermal calculations was carried out until 24:00 on 31 August. The temperature distribution determined at this moment was taken as the starting point for the entire heating season. The simulations carried out by the authors of the paper show that the form of the adopted initial condition has the greatest influence on the results obtained in the first week of calculations and to a lesser extent, on the results of the second week. On this basis, it can be concluded that the initial condition adopted was correct.

As a result of the calculations, temperature distributions in the envelope elements were obtained at individual moments of the heating period, in all analyzed cases. Sample diagrams of daily temperature variability for a building located in Poznań in January for a sunny day ($I_{sol,max}$ = 1008.2 W/m^2) and cloudy day ($I_{sol,max}$ = 66.8 W/m^2) are shown in Figure 8.

The energy balances for all analyzed cases of envelopes in the individual months of the heating season are the basic result of the simulations. These balances were obtained as a result of integration after time of heat flux density on the internal surface of the envelope. A comparison of the Q_m values obtained for the south orientation for the envelopes with transparent insulation of different thicknesses in Koszalin, Poznań, and Racibórz is shown in Figures 9–11, respectively. In the bottom part of these figures, an additional monthly average equivalent heat transfer coefficient of the envelope element U_{eq} is displayed.

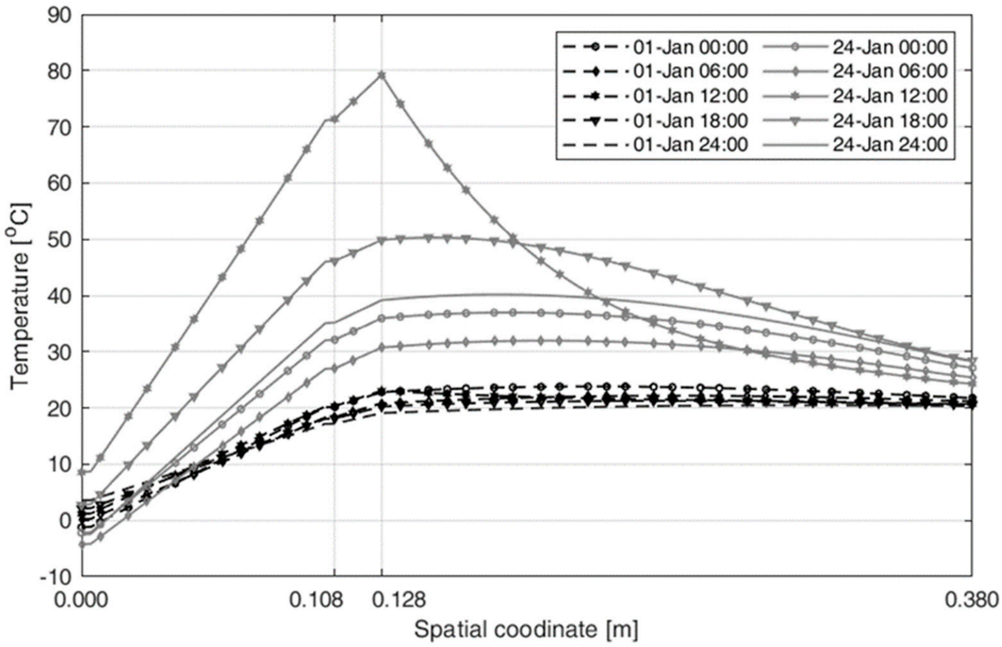

Figure 8. Changes of the temperature distribution in the envelope on a January day in Poznań (sunny day—gray lines and cloudy day—black lines).

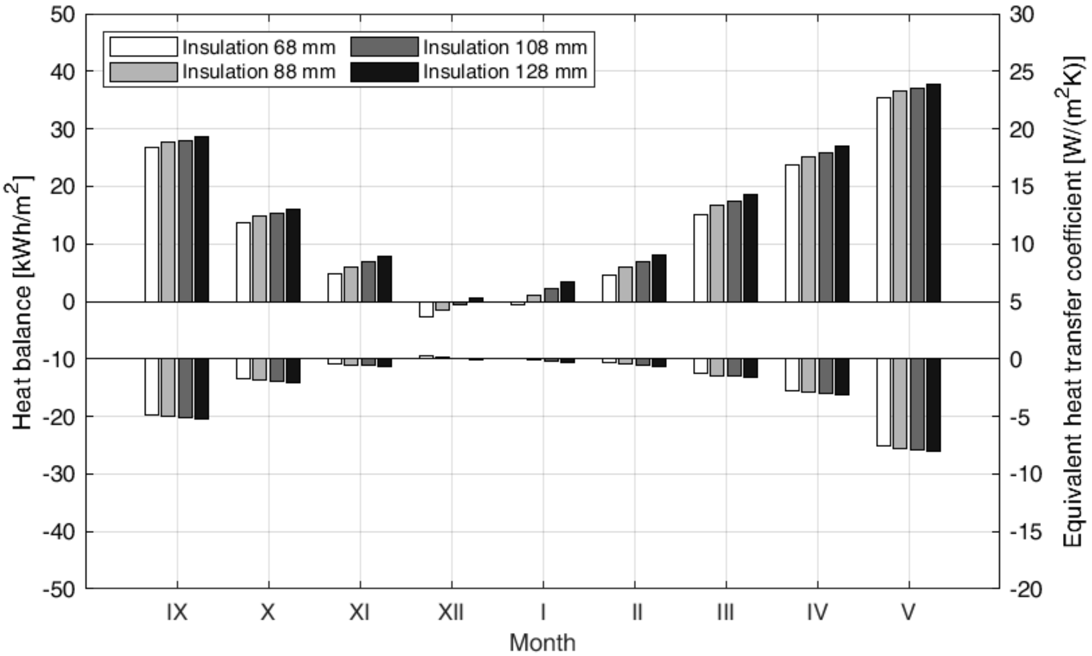

Figure 9. The Q_m (upper graph) and U_{eq} (bottom graph) values of the solar wall with transparent insulation (SW-TI) for a south orientation in the case of the application of insulation of different thicknesses (location in Koszalin).

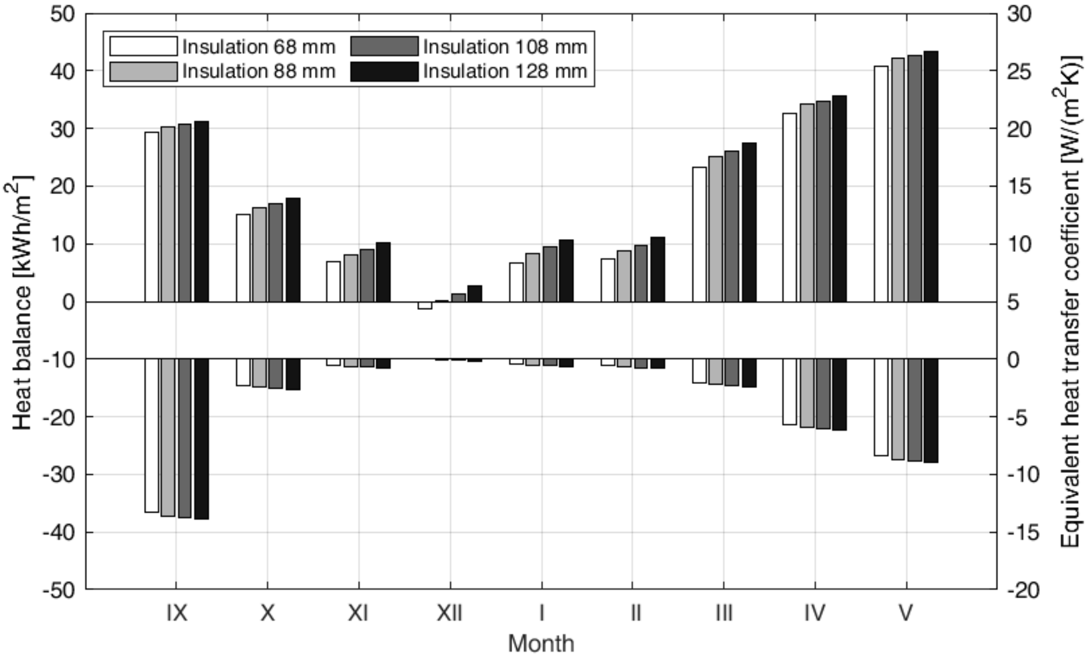

Figure 10. The Q_m (upper graph) and U_{eq} (bottom graph) values of the SW-TI for a south orientation in the case of the application of insulation of different thicknesses (location in Poznań).

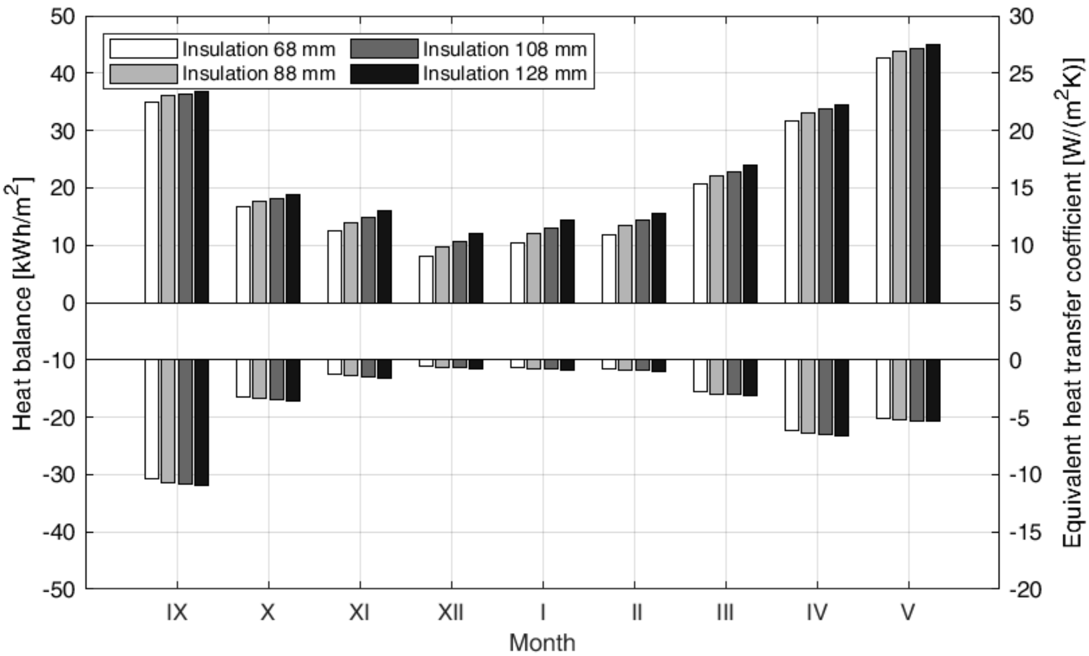

Figure 11. The Q_m (upper graph) and U_{eq} (bottom graph) values of the SW-TI for a south orientation in the case of the application of insulation of different thicknesses (location in Racibórz).

4. Discussion

The figures in point 3 show, in the case of the location of a south-oriented SW-TI wall in Koszalin, that the positive energy balance in all months of the heating season was only obtained by the envelope with transparent insulation with a thickness of 128 mm. In the case of Poznań, all positive Q_m values can be observed at the insulation thickness of 88 mm and for the thicker insulations; however, due to very low gains in December, it is advisable to use TI with a thickness of 108 mm. In the case of the location in Racibórz, i.e., in the area with the highest insolation, positive monthly energy balances were obtained for the insulations of all thicknesses.

It should be noted here that a change in insulation thickness of 20 mm does not cause large percentage changes in Q_m values and these differences decrease with the increase in sunlight. For this reason, with the change in insulation thickness from 128 to 108 mm for an envelope located in Koszalin, the annual thermal balance of Q changes by 6.10%. In the case of locations in Poznań and Racibórz, the change amounts to 5.02% and 4.15%, respectively. However, with a reduction in insulation thickness from 108 to 88 mm, the thermal balance in the individual locations changes by 4.83%, 3.9%, and 3.11%, respectively. The biggest variations are observed when the insulation thickness changes from 88 to 68 mm, at which the value of Q changes for Koszalin, Poznań, and Racibórz by 8.54%, 7.3%, and 6.13%, respectively. Therefore, the use of 68 mm thick insulation is not recommended outside areas with an annual insolation of more than 1050 kWh/m^2. However, the use of 128 mm thick insulation is only justified in areas with less than 850 kWh/m^2 of annual insolation. The most universal application in Poland seems to be the insulation thicknesses of 108 and 88 mm.

Figures 12–14 show the values of monthly thermal balances of a solar wall with a 108 mm insulation thickness for three orientations (east, south, and west), respectively, for the locations in Koszalin, Poznań, and Racibórz. The figures also show the average monthly insulation efficiency η_m.

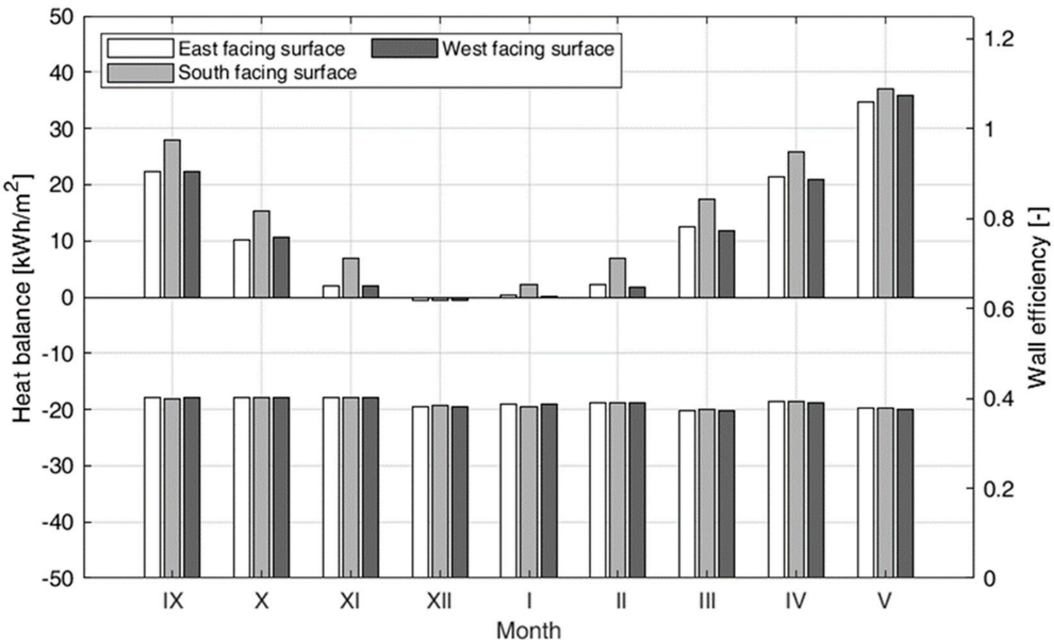

Figure 12. Comparison of monthly thermal balances (top) and thermal efficiency (bottom) of the SW-TI with the insulation thickness of 108 mm in the case of different orientations (location in Koszalin).

Additionally, in Figure 15, monthly thermal balances of the analyzed envelope for the three locations are compared. As expected, the most favorable orientation is the southern orientation of the SW-TI wall, and the change of orientation from the southern to the eastern one causes a reduction of the annual heat balance Q by 24.16% in Koszalin, 27.87% in Poznań, and 31.77% in Racibórz. On the other hand, the change of orientation from south to west reduces the annual balances of the SW-TI for the particular locations by 24.27%, 29.76%, and 30.23%, respectively. As shown by the results of the conducted analyses, the eastern and western orientations give similar values of monthly thermal balances of a solar wall (see Figures 12–14).

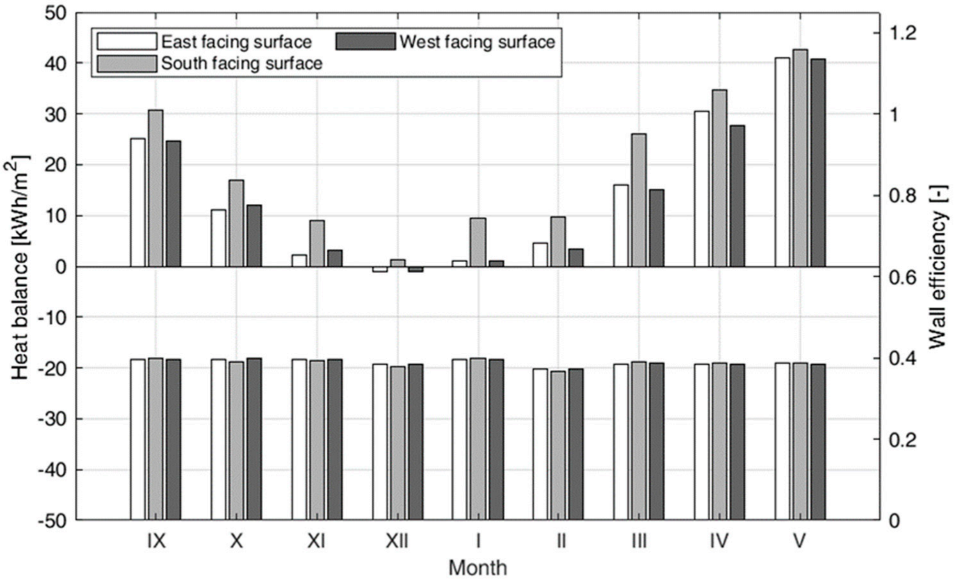

Figure 13. Comparison of monthly thermal balances (top) and thermal efficiency (bottom) of the SW-TI with the insulation thickness of 108 mm in the case of different orientations (location in Poznań).

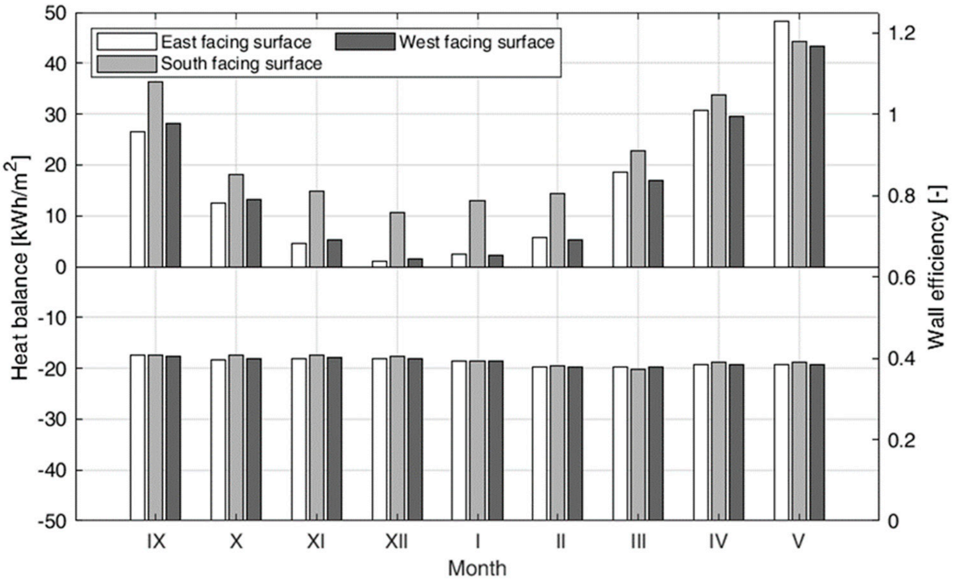

Figure 14. Comparison of monthly thermal balances (top) and thermal efficiency (bottom) of the SW-TI with the insulation thickness of 108 mm in the case of different orientations (location in Racibórz).

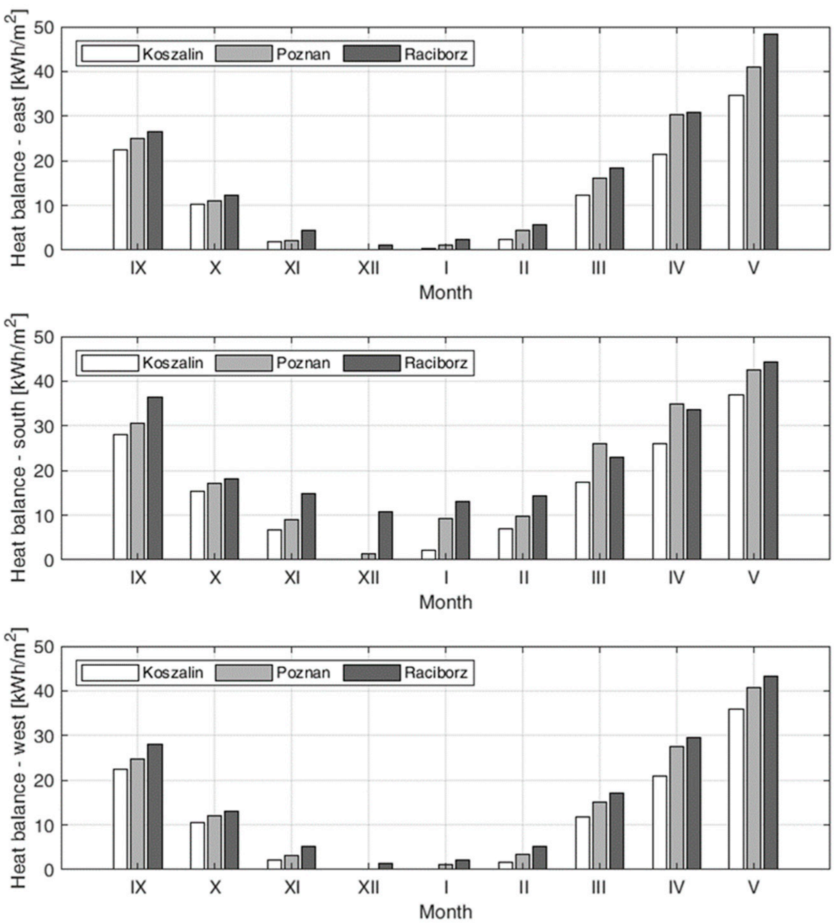

Figure 15. Comparison of monthly heat balances of an SW-TI with the insulation thickness of 108 mm located in different parts of Poland for eastern (top graph), southern (graph in the middle), and western (bottom graph) orientation.

During the calculation process, the weekly average efficiencies η of the analyzed envelope were also determined. It was found that, depending on the orientation, location, and thickness of insulation, the values of η were between 0.31 and 0.66, but in each analyzed case, the average annual TI efficiency fell within the range of 0.39 and 0.40. The values of temperatures reached at the absorber's plane and on the internal surface of the wall were also investigated. It was found, depending on the analyzed case, that the maximum temperatures on the absorber reached in the whole heating period ranged from 73.04 to 96.25 °C, whereas the internal surface of the wall heated up to 33.62 °C. Since the material of which the transparent insulation is made has a long-term thermal resistance to 100 °C, the insulation can be used in Polish climatic conditions (of course, in the case, when the transparent insulations are equipped with sunscreen roller-blinds to be used in the summer period).

The analysis of temperature distributions in the envelope showed that, regardless of the orientation of the envelope during short days in January, the maximum temperature of the absorber occurs between 12:00 noon and 1:00 p.m. The temperature wave reaches the internal surface of the envelope with a seven- and eight-hour delay and after this time, the surface reaches the maximum daily temperature. Things are different when the day gets longer. In the month of May, the maximum temperature of the east-oriented solar wall absorber occurs around 9:00 a.m. and in the west-oriented envelope, it occurs around 4:00 p.m. When designing the arrangement of transparent insulation on the facade of a building, it should therefore be borne in mind that the change of orientation of an SW-TI will cause solar gains to be delivered to the building at a different time of day. Therefore, the south and west orientations appear to be more favorable.

Within the framework of the calculations carried out, the intensity of convectional heat transport in the air gap was also investigated. It was found that the maximum density of the convection heat flux was 5.86 W/m^2 and the maximum density of the radiation flux was 90.92 W/m^2 (insulation 68 mm, Racibórz, and southern orientation). In view of the above, it was concluded that, in the case under consideration, convective heat flux within the air gap is negligible, and may be neglected during envelope modeling.

5. Conclusions

A numerical model of a solar wall with transparent insulation is proposed in this work, and it is based on the finite-difference method and the thermal conductivity equation with heat source terms. On the basis of this model and simulations performed, an energy efficiency analysis of an SW-TI was conducted in the case of different climatic conditions prevailing in Poland and different orientations of the envelope. Transparent insulation in the form of a honeycomb made of modified cellulose acetate, placed between two 4 mm glass panes (TIMax CA) of different thicknesses (68, 88, 108, and 128 mm), was applied to the wall under consideration. The following conclusions were reached:

1. In Poland, the authors recommend using 108 and 88 mm thick transparent insulation. Additionally, 68 mm thick insulation can only be used in areas with an annual insolation value of more than 1050 kWh/m^2. The use of 128 mm thick insulation is only justified in areas with less than 850 kWh/m^2 of annual insolation;
2. Placing transparent insulation on a wall with an eastern or western orientation causes the annual heat balance of the envelope to decrease by 24–31% in relation to the value of this balance in the case of a southern orientation. These differences achieve higher values in the above range for areas with higher insolation;
3. The use of transparent insulation on an eastern wall shifts the period of delivering solar gains to the rooms to afternoon hours. Such an effect is expected in September, October, April, and May. For this reason, the south-western orientation seems to be more advantageous, where the heat is supplied to the rooms regardless of the time of year, in the evening and at night;
4. The monthly thermal balances obtained using the proposed model give results consistent with the method of calculating thermal gains through opaque partitions with transparent insulation included in the PN-EN ISO 13790:2008 standard. Average differences between the values Q_m obtained from both methods range from 0.3905 to 0.8675 kWh/m^2, while the relative differences in the annual heat balance of the envelope range from 2.29% to 3.54%;
5. In the discussed case, the convective heat flux within the air gap is negligible when modelling envelope element thermal performance (weekly averaged convective heat flux densities are two to three orders lower than radiation flux densities).

Author Contributions: Conceptualization, J.Ś.-P.; data curation, J.Ś.-P.; formal analysis, J.Ś.-P.; investigation, J.Ś.-P.; methodology, J.Ś.-P.; software, J.Ś.-P.; validation, J.Ś.-P.; visualization, A.K.; writing—original draft, J.Ś.-P.; writing—review & editing, J.W. All authors have read and agreed to the published version of the manuscript.

Funding: This research received no external funding.

Conflicts of Interest: The authors declare no conflict of interest.

References

1. Harish, V.S.K.V.; Kumar, A. A review on modeling and simulation of building energy systems. *Renew. Sustain. Energy Rev.* **2016**, *56*, 1272–1292. [CrossRef]
2. Hastings, S.R. Breaking the "heating barrier": Learning from the first houses without conventional heating. *Energy Build.* **2004**, *36*, 373–380. [CrossRef]
3. Wong, I.L.; Eames, P.C.; Perera, R.S. A review of transparent insulation systems and the evaluation of payback period for building applications. *Sol. Energy* **2007**, *81*, 1058–1071. [CrossRef]

4. Ochs, M.; Haller, A.; Simmler, H.H. A simple method to calculate the heat gains of solar wall heating with transparent insulation. In Proceedings of the 3rd Int. ISES Europe Solar Congress "Eurosun 2000", Copenhagen, Denmark, 19–22 June 2000.
5. Braun, P.O.; Goetzberger, A.; Schmid, J.; Stahl, W. Transparent insulation of building facades—Steps from research to commercial applications. *Sol. Energy* **1992**, *49*, 413–427. [CrossRef]
6. Voss, K. Solar energy in building renovation—results and experience of international demonstration buildings. *Energy Build.* **2000**, *32*, 291–302. [CrossRef]
7. Dalenbäck, J.-O. Solar energy in building renovation. *Energy Build.* **1996**, *24*, 39–50. [CrossRef]
8. Kaushika, N.D.; Sharma, M.S.S. Honeycomb roof cover system for passive solar space heating. *Energy Convers. Manag.* **1987**, *27*, 99–102. [CrossRef]
9. Lien, A.G.; Hestnes, A.G.; Aschehoug, Ø. The use of transparent insulation in low energy dwellings in cold climates. *Sol. Energy* **1997**, *59*, 27–35. [CrossRef]
10. Raicu, A.; Wilson, H.R.; Nitz, P.; Platzer, W.; Wittwer, V.; Jahns, E. Facade systems with variable solar control using thermotropic polymer blends. *Sol. Energy* **2002**, *72*, 31–42. [CrossRef]
11. Wallner, G.M.; Lang, R.W.; Schobermayr, H.; Hegedys, H.; Hausner, R. Development and application demonstration of a novel polymer film based transparent insulation wall heating system. *Sol. Energy Mater. Sol. Cells* **2004**, *84*, 441–457. [CrossRef]
12. Wallner, G.M.; Hausner, R.; Hegedys, H.; Schobermayr, H.; Lang, R.W. Application demonstration and performance of a cellulose triacetate polymer film based transparent insulation wall heating system. *Sol. Energy* **2006**, *80*, 1410–1416. [CrossRef]
13. Dolley, P.R.; Martin, C.J.; Watson, D.M.J. The use of test rooms to determine the thermal performance of a transparently insulated opaque wall. *Build. Environ.* **1993**, *28*, 139–143. [CrossRef]
14. Dolley, P.R.; Martin, C.J.; Watson, D.M.J. Performance of walls clad with transparent insulation material in realistic operation. *Build. Environ.* **1994**, *29*, 83–88. [CrossRef]
15. Haller, A.; Althaus, H.-J.; Platzer, W.J.; Goerdt, W. Gain control for solar wall heating with transparent insulation (TI)–requirements for cost effective application of natural ventilation in multifunctional and ventilated façades (MFVF). In Proceedings of the 3rd Int. ISES Europe Solar Congress "Eurosun 2000", Copenhagen, Denmark, 19–22 June 2000.
16. Čekon, M.; Slávik, R. A Non-Ventilated Solar Façade Concept Based on Selective and Transparent Insulation Material Integration: An Experimental Study. *Energy* **2017**, *10*, 815. [CrossRef]
17. Čekon, M.; Čurpek, J. A transparent insulation façade enhanced with a selective absorber: A cooling energy load and validated building energy performance prediction model. *Energy Build.* **2019**, *183*, 266–282. [CrossRef]
18. Kaushika, N.D.; Sumathy, K. Solar transparent insulation materials: A review. *Renew. Sustain. Energy Rev.* **2003**, *7*, 317–351. [CrossRef]
19. Sun, Y.; Wilson, R.; Wu, Y. A Review of Transparent Insulation Material (TIM) for building energy saving and daylight comfort. *Appl. Energy* **2018**, *226*, 713–729. [CrossRef]
20. Paneri, A.; Wong, I.L.; Burek, S. Transparent insulation materials: An overview on past, present and future developments. *Sol. Energy* **2019**, *184*, 59–83. [CrossRef]
21. Yang, H.X.; Zhu, Z.L.; Burnett, J. Simulation of the behaviour of transparent insulation materials in buildings in northern China. *Appl. Energy* **2000**, *67*, 293–306. [CrossRef]
22. Heim, D. Whole year analysis of TIM-PCM solar thermal storage wall. In Proceedings of the SimBuild 2004, IBPSA, USA National Conference, Boulder, CO, USA, 4–6 August 2004.
23. Wong, I.L.; Eames, P.C.; Perera, R.S. Energy simulations of a transparent-insulated office façade retrofit in London, UK. *Smart Sustain Built Env.* **2012**, *1*, 253–276. [CrossRef]
24. Monson, W.A.; Klein, S.A.; Beckman, W.A. Prediction of direct gain solar heating system performance. *Sol. Energy* **1981**, *27*, 143–147. [CrossRef]
25. Monson, W.A.; Klein, S.A.; Beckman, W.A. The un-utilizability design method for collector-storage walls. *Sol. Energy* **1982**, *29*, 421–429. [CrossRef]
26. Dowson, M.; Harrison, D.; Dehouche, Z. Trombe walls with nanoporous aerogel insulation applied to UK housing refurbishments. *Int. J. Smart Nano Mater.* **2014**, *5*, 283–303. [CrossRef]
27. Athienitis, A.K.; Ramadan, H. Numerical model of a building with transparent insulation. *Sol. Energy* **1999**, *67*, 101–109. [CrossRef]

28. Kisilewicz, T. Glazed building wall as a solar thermal collector. *Arch. Civ. Mech. Eng.* **2009**, *9*, 83–99. [CrossRef]
29. Sá, A.B.; Boaventura-Cunha, J.; Lanzinha, J.-C.; Paiva, A. An experimental analysis of the Trombe wall temperature fluctuations for high range climate conditions: Influence of ventilation openings and shading devices. *Energy Build.* **2017**, *138*, 546–558. [CrossRef]
30. Cane, R.L.D.; Hollands, K.G.T.; Raithby, G.D.; Unny, T.E. Free convection heat transfer across inclined honeycomb panels. *J. Heat Transf.* **1977**, *99*, 86–91. [CrossRef]
31. Świrska-Perkowska, J.; Jęglet, K. Energy efficiency of the accumulation wall with a transparent insulation. In Proceedings of the 3rd Scientific Conference Environmental Challenges in Civil Engineering (ECCE 2018), MATEC Web of Conferences, Opole, Poland, 23–25 April 2018; Volume 174. [CrossRef]
32. WACOTECH/WACOSYSTEMS. Available online: https://www.wacotech.de/sonderanwendung/timax-ca/ (accessed on 19 March 2019).
33. Chwieduk, D. Solar Energy Use for Thermal Application in Poland. *Pol. J. Environ. Stud.* **2010**, *19*, 473–477.
34. Ministerstwo Funduszy i Polityki Regionalnej. Dane do obliczeń energetycznych budynków (Ministry of Funds and Regional Politics. Data for Energy Calculations of Buildings). Available online: https://www.gov.pl/web/fundusze-regiony/dane-do-obliczen-energetycznych-budynkow (accessed on 2 November 2019).
35. Salmerón, J.M.; Álvarez, S.; Molina, J.L.; Ruiz, A.; Sánchez, F.J. Tightening the energy consumptions of buildings depending on their typology and on Climate Severity Indexes. *Energy Build.* **2013**, *58*, 372–377. [CrossRef]
36. Szargut, J. *Metody Numeryczne w Obliczeniach Cieplnych Pieców Przemysłowych (Numerical Methods in Thermal Calculations of Industrial fuRnaces)*, 1st ed.; Wydawnictwo Śląsk: Katowice, Polska, 1977.
37. Defraeye, T.; Blocken, B.; Carmeliet, J. Convective heat transfer coefficients for exterior building surfaces: Existing correlations and CFD modelling. *Energy Convers. Manag.* **2011**, *52*, 512–522. [CrossRef]
38. Kaloyanov, N.; Stankov, B.; Tomov, G.; Penkova, N. Efficiency of transparent structures in Trombe walls. *J. Chem. Technol. Metall.* **2018**, *53*, 1157–1166.
39. Jelle, B.P. Solar radiation glazing factors for window panes, glass structures and electrochromic windows in buildings—Measurement and calculation. *Sol. Energy Mater. Sol. Cells* **2013**, *116*, 291–323. [CrossRef]
40. Wright, J.L. A correlation to quantify convective heat transfer between vertical window glazings. *Ashrae Trans.* **1996**, *102*, 940–946.
41. Ganguli, A.A.; Pandit, A.B.; Joshi, J.B. CFD simulation of heat transfer in a two-dimensional vertical enclosure. *Chem. Eng. Res. Des.* **2009**, *87*, 711–727. [CrossRef]
42. Bergman, T.L.; Lavine, A.S.; Incropera, F.P.; DeWitt, D.P. *Fundamentals of Heat and Mass Transfer*, 7rd ed.; John Wiley & Sons: Danvers, MA, USA, 2011.
43. ElSherbiny, S.M.; Raithby, G.D.; Hollands, K.G.T. Heat transfer by natural convection across vertical and inclined air layers. *J. Heat Transf.* **1982**, *104*, 96–102. [CrossRef]
44. PN-EN ISO 13790:2009. *Energy Performance of Buildings—Calculation of Energy Use for Space Heating and Cooling*; PKN: Warsaw, Poland, 2009.